Clays and Clay Minerals, 1973, Vol. 21, pp. 59–70. Pergamon Press. Printed in Great Britain

OPTICAL ABSORPTION SPECTRA OF CLAY MINERALS

SAMUEL W. KARICKHOFF and GEORGE W. BAILEY
Environmental Protection Agency, National Environmental Research Center – Corvallis, Southeast Environmental Research Laboratory Athens, Georgia 30601, U.S.A.

(*Received* 28 *August* 1972)

Abstract—A preliminary survey of electronic absorption spectra of clay minerals reveals the utility of u.v.-visible spectroscopy in the elucidation of structural, physical, and chemical properties of such systems. Spectra, which were obtained in the suspension, film, and single crystal states (where applicable), are interpreted in terms of iron-associated transitions. Microcrystalline clay minerals typically show Fe(III) in octahedral oxo–ligand geometry whereas mica-type minerals may show a range of iron species, including octahedral Fe(III), tetrahedral Fe(III), and octahedral Fe(II). Iron affects the local site geometry and in "high iron" minerals may dictate layer geometry and subsequently the crystalline form.

INTRODUCTION

MINERALOGISTS have historically been concerned with characterizing the chemical composition of primary and secondary minerals (i.e. clays and clay minerals) and attempting to relate variation in elemental composition with differences in the physiochemical properties of such systems. Interest in the surface chemistry of clay minerals has intensified due to the industrial importance of these systems in catalysis and on the fate, behavior and persistence of certain toxicants in the environment. With the advent of commercially-available high-resolution instruments, spectroscopy has increasingly been employed as a "window" for such characterizations and correlation investigations. I.R. studies Mortensen *et al.*, 1965; Farmer and Russell, 1967; Farmer *et al.*, 1968; White, 1971; and Mössbauer; Weaver *et al.*, 1967; Taylor *et al.*, 1968; Bowen *et al.*, 1969; have certain distinct inadequacies. For example, they are restricted to relatively dry systems and structural characteristics and inferred chemical behavior cannot be easily extrapolated to wet systems. Infrared spectroscopy applied to clay mineral systems is a highly empirical method (Farmer *et al.*, 1968); spectral complexity defies exact theoretical analysis. Mössbauer spectroscopy is restricted essentially to iron monitoring and therefore cannot be used in characterizing clay structure and surface chemistry extraneous to iron.

Electronic optical spectroscopy until recently has been essentially neglected as a tool in studying and characterizing clay mineral systems. Ultraviolet spectroscopy has advantages not found in i.r. or Mössbauer: (1) spectra can be easily taken in either wet or dry systems, (2) both the structure and chemistry of clay minerals can be studied in either state, (3) the spectra are inherently simple, thus facilitating theoretical deciphering and band assignment.

Reported electronic optical spectroscopic studies of either primary minerals or clay minerals are sparse. Micas have been studied extensively by Faye (1968a) and Faye *et al.* (1970) in the visible and near i.r. regions. Faye assigned the spectral structure in micas, but the electronic spectra of clay minerals have not been reported. Bergmann and O'Konski (1963) noted, in their spectroscopic study of methylene blue adsorbed on montmorillonite, a background u.v. band in the clay peaking at 242 nm. Banin *et al*, (1968) utilized electronic spectroscopy to correlate the effect of cationic character of montmorillonite with tactoid size. He reported a similar band for montmorillonite but attributed it to an organic impurity.

Our work characterizes the electronic spectra of a variety of clay minerals and certain primary minerals, and attempts to correlate chemical composition with certain structural and electronic properties, We intend this contribution not as a comprehensive treatise, but only as a preliminary survey of the optical properties of the minerals. Such a study is a prerequisite, however, to correlating chemical compositions and structure with the adsorptive-desorptive and surface acidity properties of clay minerals.

SPECTRAL THEORY

The basic "building blocks" of the clay lattice (gibbsite, brucite, quartz) do not absorb light in the frequency range studied (195–800 nm). Absorption in this region results from the presence of

transition-metal cations—either as structural elements within the lattice or as exchangeable cations on the surface. Clay minerals are endowed with trace amounts of a multitude of transition metals, but in the systems studied (Table 1), the electronic transitions leading to light absorption in the u.v. and visible regions were almost without exception connected with the presence of iron. Minor contributions arise from titanium, but the gross spectral features are due to Fe(III) and Fe(II).

This discussion of theoretical concepts is directed toward iron cations in the mineral lattice, but the same principles would apply to other cations. Spectral characteristics can best be subdivided on the basis of the nature of the electronic transition associated with light absorption. The two distinct types of transitions evident in mineral spectra are intraconfigurational and charge transfer. "Intraconfigurational" refers to transitions between levels belonging to the same electronic configuration, whereas "charge transfer" refers to what is often described as a partial migration of an electron from one nuclear center to another.

Intraconfigurational electronic transitions

Intraconfigurational transitions occur as a result of d electrons in an unfilled $3d$ shell (Fe(II) has a d^6 electron configuration, Fe(III) is d^5). These electrons are subject primarily to three competing interactions:

(a) electron correlation or electron-electron repulsion (V_{ee}).
(b) spin-orbit coupling (V_{so}).
(c) electron-ligand interactions (V_{el}).

In clay mineral systems the ligands are all oxo in nature (i.e. 0^{2-}, OH^-, OH_2) and have similar spectroscopic behavior. For the iron–oxo system the relative effects of the aforementioned interactions on the energetics of the d^n ($n = 5,6$) electron configuration are:

$$V_{ee} > V_{el} > V_{so}.$$

An energy level scheme is developed by considering these perturbations on the d^n configuration in the order of their relative importance. This scheme

Table 1. Description of minerals used

Material	Physical Description	Geographic origin (if known)
Montmorillonite # 21 (Wards)	yellow–white powder	Polkville, Mississippi
Montmorillonite # 22A		Amory, Mississippi
Montmorillonite # 24		Otay, California
Montmorillonite # 25		Upton, Wyoming
Montmorillonite # 31		Cameron, Arizona
Nontronite # 33A (Wards)*	yellow powder	Garfield, Washington
Sepiolite	white powder	
Hectorite # 34		Hector, California
Beidellite (Wards)*		Fort Sandeman, Pakistan
Halloysite # 12		Bedford, Indiana
Kaolinite # 4 (Wards)		Macon, Georgia
Attapulgite		Attapulgus, Georgia
White Store Soil Clay (B_2)†	orange–white powder	North Carolina
Iredell Soil Clay (B)‡	gray powder	Virginia
Berks Soil Clay (B)‡	orange–white powder	Virginia
Cecil Soil Clay (A_1)§	red–brown powder	South Carolina
Phlogopite A (Wards)	amber sheets	Ontario
Phlogopite B (North Burgess, Wards)		Ontario
Muscovite (Wards)	green–black sheets	Effingham T.W.P., Ontario
Vermiculite	yellow flakes	Transvaal
Biotite	green–black sheets	Bancroft, Ontario

*Nontronite and Beidellite were obtained from Dr. S. B. Weed, N. C. State Univ.
†White Store was obtained from Dr. S. W. Buol, N. C. State Univ.
‡Iredell and Berks were obtained from Dr. C. I. Rich, Virginia Polytechnic Institute and State Univ.
§Cecil was obtained from Dr. T. C. Peele, Clemson Univ.

can be represented diagrammatically by

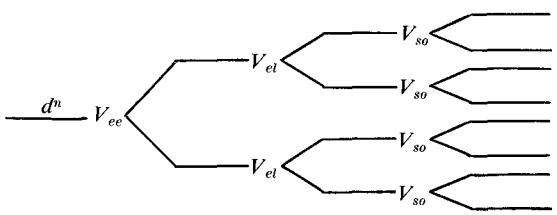

Thus, the manifold of degenerate microstates of the d^n configuration (corresponding to different permutations of the n electrons in the ten $3d$ orbitals) is split into a series of states, each corresponding to a single microstate or a given combination of microstates. The methodology for developing such an energy level scheme is manifested in crystal field theory (Lever, 1968). The procedure used here to analyze clay mineral spectra is not to calculate the spectrum *a priori*, but rather to compare the spectral features to those of simpler iron-oxo systems wherein the metal valence state and ligand symmetry are known. The spectra ised for reference were taken from the following works:

(a) u.v.-visible spectra of Fe(III) doped into numerous oxo inorganic salts (Lehmann, 1970).
(b) visible spectra of Fe(II) complexes in solution (Furlani, 1957).
(c) visible spectra of micas (Faye, 1968, a,b; Faye *et al.*, 1970).

Charge transfer transitions

The clay mineral systems described herein show primarily three types of charge transfer transitions: ligand to metal; metal to ligand; and metal to metal. Metal–ligand transfer occurs as a result of overlap of donor and acceptor orbitals. Metal–metal transfer can occur as a result or overlap of the metal orbitals involved or via intermediate ligand states (virtual process). Any calculation of transition energies from a crystal field model (or any modification thereof) is very difficult and no single method has met with widespread success. One of the simpler and perhaps more successful approaches is to describe transition energies in terms of three relatively simple electrostatic terms,

$$E_{ct} = E_D - E_A + \Delta V.$$

The precise meaning of each term varies depending upon the system under investigation, but generally speaking, E_D is some measure of the energy required to pull an electron off the donor species; E_A is indicative of the energy released by the acceptor species when it accepts an electron; ΔV is the corrective term that is generally related to the change in the electrostatic donor-acceptor interaction effected by charge transfer. For anion donors and cation acceptors, ΔV varies inversely with R_{DA}, where R_{DA} denotes the interionic separation.

Jorgensen's approach (1962a,b) utilizes an equation similar to the electrostatic equation, but wherein each term is defined in terms of spectroscopic parameters, i.e. $E_D(E_A)$ refers to the so-called "optical electronegativity" of the donor (acceptor) orbitals involved; ΔV refers to a change in interelectronic repulsion effected by charge transfer. Jorgensen has tabulated these electronegativities for many common ligands and transition metals in various valence states and ligand geometries (see Lever, 1968). Charge transfer spectra are also analyzed by comparison with spectral works in iron–oxo systems (listed previously).

EXPERIMENTAL

Electronic spectra were obtained using several techniques depending upon the crystallographic state of the mineral (Table 1). Spectra of microcrystalline materials were obtained in both the film and suspension. The original materials were fractionated to less than 2 μm particle size by sedimentation and homoionically saturated (where indicated) with metal cations according to Bailey *et al.* (1968). The resulting suspensions were then sonicated (1000 W). Films were prepared by placing 1 ml aliquots on quartz discs and allowing the samples to air dry. The spectra of the sheet minerals (micas and vermiculite) were run in the single crystal state. The original materials were cleaved into thin crystals, uniform in thickness and color. Approximate thicknesses were determined with a micrometer.

All spectra were recorded on a model 356 Perkin–Elmer u.v.-Vis spectrophotometer* employing multiple detector tubes (R-473 and R-375 tubes in the visible region, R-189 tube in the u.v. range).

The single crystals and films were mounted in the spectrometer approximately 2 mm from the front of the detector-tube casing to minimize scattered-light losses. For single crystal spectra, air was used as the reference and for films, a quartz disc was used. Suspensions were run in quartz cells (1 cm path length) placed approximately 5 mm from the phototube; here, water was

*Reference to trade names and commercial products is for information only and does not constitute endorsement by the Environmental Protection Agency.

https://doi.org/10.1346/CCMN.1973.0210109 Published online by Cambridge University Press

used as the reference. All spectra were recorded in the absorbance mode at room temperature using unpolarized light.

DESCRIPTION OF SPECTRA

Smectites

Smectites occur only as very small particles, therefore single crystal electronic spectra cannot be obtained. Suspensions and thin film spectra show a high degree of light scattering which tends to mask any intra-configurational structure. Only in iron-rich nontronite does the visible region contain any spectral structure; however, the ultraviolet spectrum contains transitions revealing the presence (in a semi-quantitative way), the site of substitution, and the valence state of the iron in the lattice.

Montmorillonites characteristically show a charge transfer transition in the 241–243 nm range in both the film and suspension (Figs. 1 and 2) independent of the geographical source and saturating cation. There seems to be a second transition in the range 191–195 nm but the intense background makes a definite location of this band difficult. Both transitions are assigned to charge transfer (oxo–Fe(III) octahedral). The position and separation of the bands agree well with Lehmann's observations of iron (III) in oxo salts. In general, the relative absorbances of different montmorillonites reflect the number of iron centers available to the light and amount of incident light lost by scattering. Montmorillontes saturated with divalent cations show a generally reduced absorbance and reduced resolution compared to their monovalent counterparts (Fig. 2). In suspension, montmorillonites saturated with divalent metal cations form tactoids

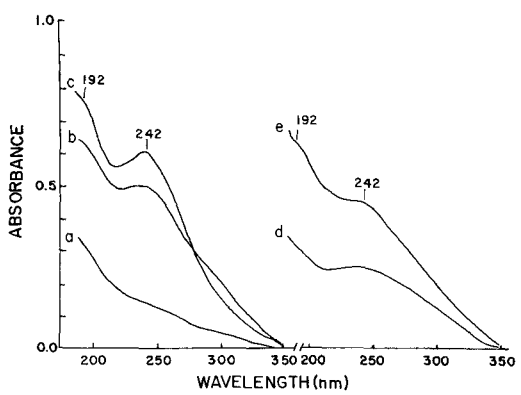

Fig. 1. U.V. spectra of standard montmorillonites – native saturation. a. Montmorillonite # 24 film (0·20 mg/cm²). b. Montmorillonite # 22a film (0·25 mg/2 cm²). c. Montmorillonite # 25 suspension (0·24 mg/ml). d. Montmorillonite # 31 suspension (0·28 mg/ml). e. Montmorillonite # 21 film (0·25 mg/cm²).

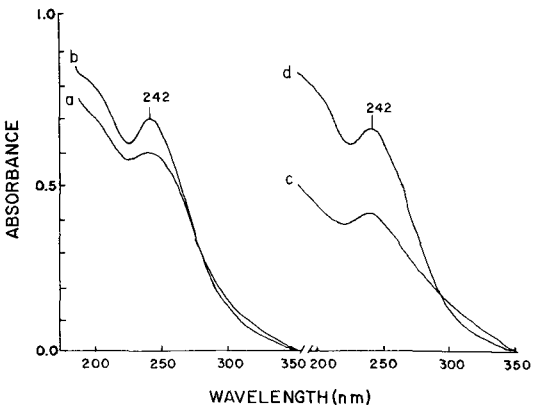

Fig. 2. U.V. spectra of montmorillonite # 25 as a function of saturating cation. a. Ca Montmorillonite film (0·25 mg/cm²). b. K Montmorillonite film (0·25 mg/cm²). c. Mg Montmorillonite suspension (0·27 mg/ml). d. Na Montmorillonite suspension (0·28 mg/ml).

which have a high degree of randomness in the relative orientation of the microcrystalline basal planes. This tactoid structure increases light scattering and also renders more absorbing sites inaccessible to the light. Increased scattering tends to increase the apparent absorbance of the medium whereas the shielding of light-absorbing sites tends to decrease absorbance. In montmorillonites saturated with divalent metal cations, the shielding effect dominates the scattering effect, leading to reduced absorbance over the monovalent counterparts. Also, increased scattering coupled with shielding leads to a loss of spectral resolution in the divalent systems. There is also a cation mass effect on the absorbance of a given montmorillonite saturated with various cations. However, in comparing Na–montmorillonite to Mg–montmorillonite or comparing *K*–montmorillonite to Ca–montmorillonite, this mass effect can be neglected.

Nontronite shows not only the u.v. charge transfer bands attributable to octahedral iron (III), but also shows, in films and suspensions, intraconfigurational transitions in the visible region (Fig. 3). Table 2 contains a summary of these transitions and assignments. For the iron (III)–oxo complex, the ground state (corrected for electron correlation, V_{ee}) is ^6S which is unsplit by the crystal field interaction, V_{et}. All intraconfigurational structure involves spin-forbidden transitions to spin quartet states; the assignment notation used in Table 2 and throughout this paper involves Mulliken symbols (Lever, 1968) denoting states which have not been corrected for spin-orbit coupling, V_{so}.

Beidellite and hectorite show essentially no absorption throughout the spectral regions studied

https://doi.org/10.1346/CCMN.1973.0210109 Published online by Cambridge University Press

Table 2. Nontronite spectral summary

Octahedral Iron (III) Max (nm)	Description	Assignment
520	broad shoulder	$^4T_2(G) \leftarrow {}^6A_1(S)$
445	strong shoulder	$^4A_1{}^4E(G) \leftarrow {}^6A_1(S)$
384	weak shoulder	$^4T_2(D) \leftarrow {}^6A_1(S)$
367	moderate shoulder	$^4E(D) \leftarrow {}^6A_1(S)$
262	very strong band	charge transfer oxo → iron (III) (oxtahedral)
200	very strong band	charge transfer oxo → iron (III) (octahedral)

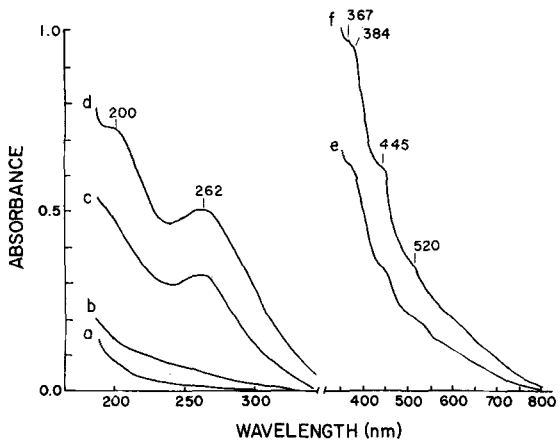

Fig. 3. U.V.—vis spectra of other smectites—Na saturated. a. Hectorite suspension (0·30 mg/ml). b. Beidellite suspension (0·25 mg/ml). c. Nontronite suspension (0·03 mg/ml). d. Nontronite film (0·02 mg/cm²). e. Nontronite film (0·50 lg/cm²). f. Nontronite suspension (1·0 mg/ml).

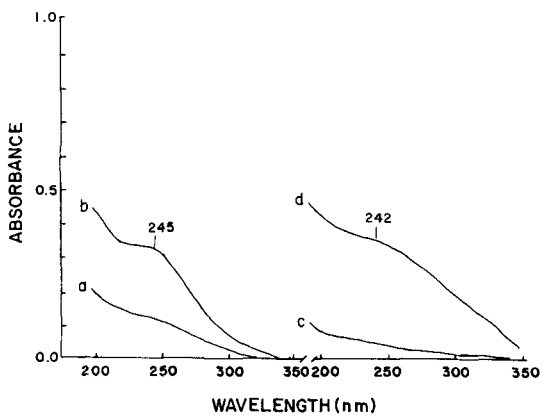

Fig. 4. U.V. spectra of sepiolite, attapulgite; halloysite, and kaolinite—no cationic saturation. a. Sepiolite suspension (0·26 mg/ml). b. Attapulgite suspension (0·25 mg/ml). c. Halloysite film (0·25 mg/cm²). d. Kaolinite film (0·25 mg/cm²).

(Fig. 3), which is indicative of low iron levels in the lattice.

Neither iron (II) or tetrahedrally coordinated iron (III) were evidenced in the smectite spectra, and all the octahedrally coordinated iron (III) was in dioctahedral systems.

Kaolinite, halloysite, sepiolite, attapulgite

Just as in the smectites, all of these minerals were studied in both the film and suspension. None of them show any spectral structure in the visible region so only the u.v. spectra are reproduced in Fig. 4.

Kaolinite shows a very weak shoulder in the 240 nm region, assigned (as in the smectites) to charge transfer (oxo to iron (III) octahedral). The large crystalline particle size shields many of the internal lattice sites from the light and also results in appreciable scattering. However, a trace amount

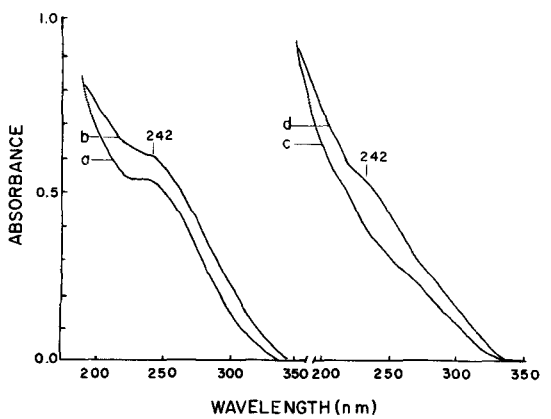

Fig. 5. U.V. spectra of soil clays—native saturation. a. White store suspension (0·25 mg/ml). b. Iredell suspension (0·25 mg/ml). c. Berks film (0·25 mg/cm²). d. Cecil film (0·25 mg/cm²).

of octahedral iron (III) (< 1%) seems to be present.

Halloysite shows only light scattering with no resolved structure, again indicative of low iron levels.

Sepiolite has a weak 240 shoulder but as in kaolinite, scattering dominates the spectrum.

Attapulgite has a band at 245 nm (comparable in intensity to the montmorillonites) which is indicative of an octahedral iron (III) content in the 2–3 per cent range.

Mica minerals

Micas are well crystallized long-range ordered minerals which can be easily cleaved to yield very thin flakes, well suited for spectroscopic study in the single crystal state. Iron is abundant in most of these minerals and single crystal spectra make the study of intraconfigurational as well as charge transfer transitions possible. Faye has studied electronic transitions in micas primarily in the visible and near infrared spectral ranges (Faye, 1968a, b; Faye and Nickel, 1970). The spectra presented here extend these studies into the u.v. region and complement the visible region studies. Spectral summaries and assignment schemes are given in Table 3.

In muscovite, the visible spectrum shows primarily iron (III) in the octahedral layer. The spectrum is very similar to that published by Faye (1968). Muscovite crystals could not be cleaved into sections thin enough to obtain well-resolved u.v. spectra; however, features attributed to both iron (II) and iron (III) are present.

In phlogopite *A* the u.v. and visible spectra show iron (III) in tetrahedral coordination (Fig. 8). Lehmann's (1970) u.v. and visible spectra of iron (III) in tetrahedral oxo geometry in inorganic salts are very similar to that of phlogopite *A*. Phlogopite *B* shows no intraconfigurational structure, but two broad shoulders at 415 nm and 275 nm are present which are undoubtedly of charge transfer origin (Fig. 6). Faye (1968,a) observed similar structure in some phlogopites and attributed the transitions to charge transfer from Fe(II) to Ti(IV) (415 nm) and Al(III) (275 nm).

The biotite u.v. and visible spectra are dominated by charge transfer transitions which nearly mask all intraconfigurational structure (Fig. 7). As in muscovite, biotite cannot be cleaved into sections thin enough to permit good resolution of the u.v. structure. The octahedral iron (II) intraconfigurational bands were assigned by comparison of the spectrum to that of $Fe(H_2O)_6+2$ (Furlandi, 1957). The charge transfer bands were assigned according to Faye (1968,a).

Table 3. Mica spectral Summary

max (nm)	description	assignment
	Muscovite	
Octahedral iron (III)		
579	weak, broad band	$^4Ti(G) \leftarrow {}^6A_1(S)$
523	weak, broad band	$^4T_2(G) \leftarrow {}^6A_1(S)$
503	weak, broad band	
441	strong shoulder	$^4A_1{}^4E(G) \leftarrow {}^6A_1(S)$
379	weak shoulder	$^4T_2(D) \leftarrow {}^6A_1(S)$
363	moderate shoulder	$^4E(D) \leftarrow {}^6A_1(S)$
242	broad shoulder	charge transfer oxo → Fe (III) (octahedral)
Octahedral iron (II)		
402	very weak shoulder	$^3E_g{}^3T_1 \leftarrow {}^2T_2$
275	broad shoulder	charge transfer Fe (II) → Al (III)
	Phlogopite A	
Tetrahedral iron (III)		
525	weak shoulder	$^4T_1(G) \leftarrow {}^6A_1(S)$
489	weak shoulder	$^4T_2(G) \leftarrow {}^6A_1(S)$
443	strong shoulder	$^4A_1{}^4E(G) \leftarrow {}^6A_1(S)$
410	weak shoulder	$^4T_2(D) \leftarrow {}^6A_1(S)$
380	very weak shoulder	$^4E(D) \leftarrow {}^6A_1(S)$
212	very strong band	charge transfer oxo → Fe (III) tetrahedral
	Phlogopite B	
425	very broad shoulder	charge transfer Fe (II) → Ti (IV)
280	very broad shoulder	charge transfer Fe (II) → Al (III)
	Biotite	
Octahedral iron (II)		
704	broad shoulder	charge transfer Fe (II) → Fe (III)
482	weak shoulder	$^3T_1 \leftarrow {}^5T_2$
456	weak shoulder	$^3T_2 \leftarrow {}^5T_2$
400	moderate shoulder	$^3Eg, {}^3T_1 \leftarrow {}^5T_2$
385	weak shoulder	$^3T_2 \leftarrow {}^5T_2$
270	broad strong shoulder	charge transfer Fe (II) → Al (III)

Vermiculite

The vermiculite spectrum is dominated by Fe (III) in two different substitution sites, octahedral and tetrahedral (Fig. 8). A spectral summary and tentative assignments are given in Table 4.

The last sets of iron (III) bands could have resulted from spectral splitting due to distorted ligand symmetry but this was ruled out because of the lack of significant splitting in other iron (III)–oxo systems. Part of the spectral structure could be indicative of interlayering; the 704 nm band could

https://doi.org/10.1346/CCMN.1973.0210109 Published online by Cambridge University Press

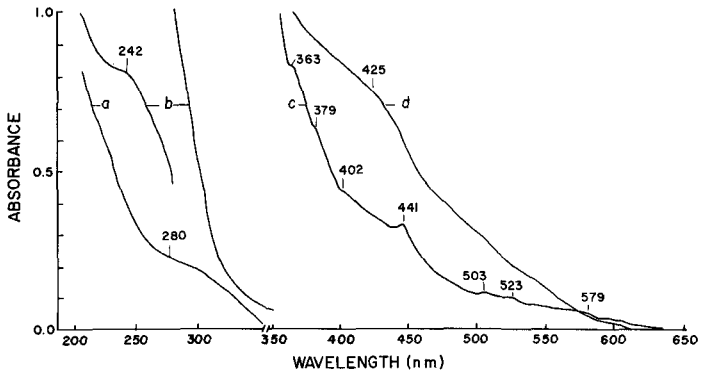

Fig. 6. U.V.–vis spectra of muscovite and phlogopite *B*. a. Phlogopite *b* sheet (~ 0·005 cm). b. Muscovite sheet (~ 0·001 cm). c. Muscovite sheet (~ 0·080 cm). d. Phlogopite *B* sheet (~ 0·017 cm).

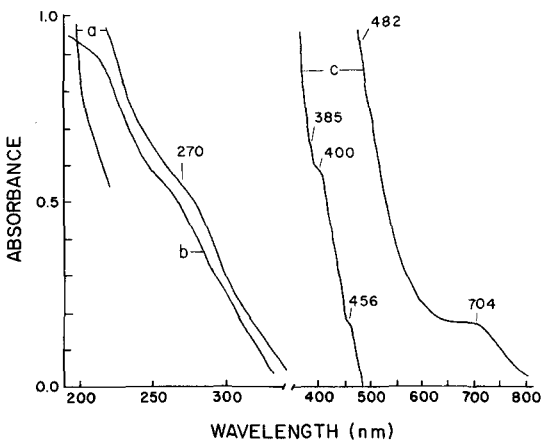

Fig. 7. U.V.-vis spectra of biotite and illite. a. Biotite sheet (~ 0·001 cm). b. Illite film (0·25 mg/cm²). c. Biotite sheet (~ 0·006 cm).

Table 4. Vermiculite spectral summary

max (nm)	description	assignment
Octahedral Fe (III)		
600	weak band	$^4T_1(G) \leftarrow {}^6A_1(S)$
575	weak band	
540	weak shoulder	$^4T_2(G) \leftarrow {}^6A_1(S)$
460	strong shoulder	$^4A_1{}^4E(G) \leftarrow {}^6A_1(S)$
400	weak shoulder	$^4T_2(D) \leftarrow {}^6A_1(S)$
250	very strong shoulder	charge transfer oxo → Fe (III) (octahedral)
Tetrahedral Fe (III)		
523	weak shoulder	$^4T_1(G) \leftarrow {}^6A_1(S)$
487	weak shoulder	$^4T_2(G) \leftarrow {}^6A_1(S)$
440	weak shoulder	$^4A_1(G) \leftarrow {}^6A_1(S)$
411	weak shoulder	$_4T_2(D) \leftarrow {}^6A_1(S)$
704	broad weak band (biotite impurity)	charge transfer Fe (II) → Fe (III)

result from traces of biotite present and the tetrahedral iron (III) could be indicative of interlayered phlogopite.

Soil clays

The spectroscopic behavior of soil clays is essentially that of their basic clay mineral constituents (Fig. 5). Iredell and White Store behave as montmorillonite spectroscopically, whereas Cecil and Berks behave as their respective clay mineral counterparts, kaolinite and illite. In general, the soil clays show increased light scattering and less resolution than their mineral constituents even at particle sizes smaller than 0·08 μm. This may be due to amorphous metal oxide and hydroxide constituents.

DISCUSSION OF INTRACONFIGURATION SPECTRA

Intraconfigurational spectral structure can be resolved in nontronite, vermiculite and several micas. This information coupled with u.v. data can be used in "fingerprinting" the iron in the lattice. Information pertaining to ligand-metal bonding and distortions from regular ligand geometry can also be obtained. An in-depth spectral analysis presupposes an accurate knowledge of transition energies, bandwidths and extinction coefficients, which are difficult to obtain for these systems since the intraconfigurational structure is superimposed on a very intense charge transfer background. However, within the framework of the spectra presented here and the works of Lehmann and Faye, several observations are noteworthy.

https://doi.org/10.1346/CCMN.1973.0210109 Published online by Cambridge University Press

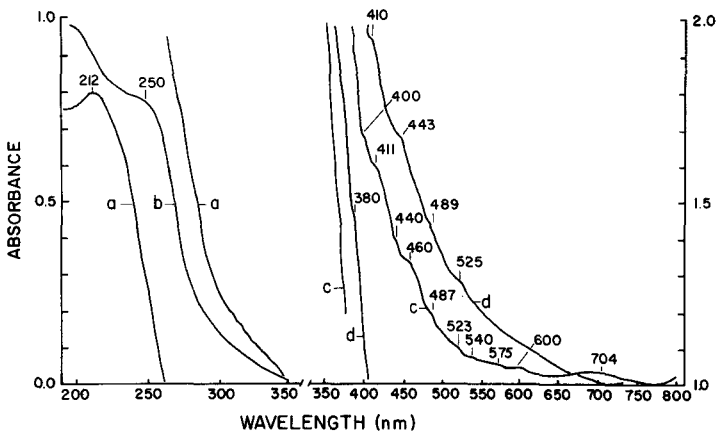

Fig. 8. U.V.-vis spectra of phlogopite *A* and vermiculite. a. Phlogopite *A* sheet (~ 0·001 cm). b. Vermiculite flake (~ 0·005 cm). c. Vermiculite flake (~ 0·010 cm). d. Phlogopite *A* sheet (~ 0·007 cm).

Within the context of the basic crystal field model, all the intraconfigurational transitions of d^5 Fe(III) and d^6 Fe(II) appearing in the visible and ultraviolet spectra are both spin and Laporte forbidden, and are therefore expected to be extremely weak. The spin selection rule is relaxed by spin-orbit coupling to the extent that transitions corresponding to a reduction of total cation spin by one unit are observed, e.g. for Fe(III), transitions from spin sextets to spin quartets; for Fe(II), transitions from quintets to triplets. However, extinction coefficients (0·1-cm²/mmole, Lehmann) tend to be as much as two orders of magnitude greater than expected from a purely crystal field standpoint. Therefore, a mechanism for relaxing the orbital (Laporte) selection rule must be rationalized. The most significant omission of the crystal field model as it pertains to these systems is the neglect of ligand–metal orbital mixing. The ramifications of this mixing that lead to intensity enhancement are: formation of iron–oxo–iron bridges; "intensity stealing" from charge transfer states; and increased covalency of iron–oxo bonds.

Iron–iron coupling via oxygen bridges relaxes local site symmetry restrictions, thus producing significant intensity enhancement. This effect is no doubt important in high-iron nontronite; a similar effect has been noted in the case of d^5 Mn(II) (McClure, 1963).

In these minerals, the most important consequence of orbital mixing (so far as intensity enhancement is concerned) is the resultant incorporation of charge transfer character into the *d* electronic states. The resultant spectroscopic behavior is commonly termed "intensity stealing" and is quite evident in these mineral spectra. This state-mixing varies inversely with the energy separation of the states involved. This inverse variation is reflected in all the intraconfigurational spectra in that the intensity of the transitions tends to drop off as the distance (energy separation) from the intensity-donating charge transfer band increases. Also, Faye (1968) notes that some of the *d* transitions in chlorite reflect the polarization character of the charge transfer states, indicative of intensity stealing.

Metal–ligand orbital mixing also gives a certain degree of covalency to the metal–ligand bond. Although the degree of covalency is small (15–20 per cent), the resultant intensity enhancement can be appreciable. Lehmann (1970) found roughly an exponential dependence of intensity on the degree of covalency.

Spectral diffuseness or large transition bandwidths are exhibited in all the spectra. This is due in part to metal–ligand orbital mixing which associates new degrees of freedom with every *d* electronic transition. Diffuseness can also be the result of crystallographic heterogeneity which is of three basic types:

(a) Nonequivalence of the actual ligand species (O^{-2}, OH^-, OH_2).
(b) Nonequivalence of different substitution sites in a given layer.
(c) Distortion of the local site from regular ligand geometry.

The octahedral iron (III) intraconfigurational transition energies vary in the order: vermiculite < nontronite < muscovite. This variation reflects a correlation with hole size (the effective lattice

https://doi.org/10.1346/CCMN.1973.0210109 Published online by Cambridge University Press

volume available for the Fe(III) cation), i.e. the larger the substitution hole, the lower the transition energy. Increasing the hole size results in decreased level splitting due to electron correlation, V_{ee}. Thus, the field independent states ^4A, $^4E(G)$ and $^4E(D)$, decrease in energy with increased hole size. The crystal field splitting effected by V_{el} also decreases with increased hole size (Orgel, 1957), so the energy of field-dependent states depends on the change in level splittings effected by both V_{el} and V_{ee}. However, in general, the transition energies observed in these spectra decrease with increasing hole size. A similar trend is observed in the charge transfer spectra which are discussed later.

The relative hole sizes can be rationalized thus: in muscovite the hole available to the Fe(III) is roughly the cationic volume of Al(III) since Fe (III) is substituted into a layer which is predominantly of the gibbsite type. In nontronite, which contains nearly all Fe (III) in the octahedral layer, the hole size is roughly the Fe(III) cation volume. In vermiculite the hole size is expected to be approximately the volume of the Mg(II) cation. On the basis of ionic radii, the relative size of the holes available to Fe(III) should be:

Al(III) (muscovite) < Fe(III) (nontronite) ~ Mg(II) (vermiculite) This is the general trend observed; however, the Fe(III) cationic volume in vermiculite appears to be somewhat larger than would be expected on the basis of the ionic radii of the host cations. A possible explanation of this discrepancy may be found in vermiculite genesis. In the mica precursor of vermiculite, the octahedral Fe(III) sites were occupied by larger Fe(II) cations, which may have distorted the surrounding ligands producing an enlarged cationic lattice hole which did not relax completely to the Mg(II) cationic volume upon oxidation of the Fe(II) in for formation of vermiculite.

Several characteristics concerning local site symmetry can be inferred from these spectra. Slight geometric distortion from regular symmetry contributes to band broadening, but can also produce spectral splitting. These distortions can arise from either "external" crystallographic forces or "internal" inner complex electronic forces. In mineral systems, crystallographic forces lead to distortions around the Si(IV), Al(III), and Mg(II) cations, but the iron cations seem much less susceptible to these crystallographic effects. The spectra show very little crystallographic distortion from regular symmetry around the iron cations. Iron (III) (d^5) complexes have a near spherical d-electronic distribution and are therefore not very susceptible to "internal" distortion forces. In minerals, iron (III)–oxo geometry tends toward regular geometry. That is, the local site geometry tends to be more regular in symmetry than that of the host. Inner-complex forces tend to negate the crystallographic distortion effects; the greater the iron content, the lesser the distortion from regular ligand geometry around the iron cations. In "low iron" muscovite and vermiculite, the iron (III) shows some distortion from regular octahedral geometry as evidenced by the splitting of some of the lower d levels. However, in "high iron" nontronite, the inner complex forces seem to dictate the local geometry; no significant distortion is evident in the spectra. The octahedra appear regular although the octahedral layer is no doubt expanded compared to gibbsite geometry.

Iron (II) complexes are more susceptible to inner-complex distortion forces (i.e. Jahn–Teller). Faye (1968) has described Jahn–Teller splitting of the $^5E_g(D)$ state of iron (II) in biotite. Here again the crystallographic effects on site geometry around the iron cations are not as significant as might be expected.

DISCUSSION OF CHARGE TRANSFER TRANSITIONS

Ligand–metal (oxo–iron III)

All mineral systems containing iron (III) in the lattice show charge transfer which can be attributed to "effective" migration of an electron (via photon perturbation) from an oxo ligand to an iron (III) cation. Spectra of dioctahedral clay minerals containing iron (III) substituted for aluminum show an intense, usually well resolved band in the range 240–245 nm; a second somewhat ill-defined band appears in the region 190–195 nm. In nontronite, where aluminum is almost totally replaced by iron (III), these transitions are shifted considerably to lower energies (262 nm, 200 nm). The spectra of trioctahedral clay minerals containing iron (III) substituting for magnesium show a band in the range 245–250 nm; the second band is either absent or lost in the intense background. Tetrahedral iron (III) minerals show but one transition – that coming around 215 nm.

The energy variation of the charge transfer transition oxo to iron (III) (octahedral) is probably due in part to variations in the average ligand–metal distances in the various mineral lattices. According to the crude electrostatic theory presented previously, increasing the average ligand–metal distance would decrease the charge transfer energy. Qualitatively, at least, the downfield shift observed for iron (III) substituted in the brucite-type layer could be due to expanded brucite geometry (relative to gibbsite-type structure). This expansion effect could also contribute to the downfield shift in nontronite.

In nontronite, however, another factor affects the transition energy. Iron (III) neighbors can couple either directly or via oxygen bridges. Each iron center looses its individual identity as far as its reaction to a photon field is concerned. Instead of localized charge transfer states, exciton states are realized which picture the transitory partial "photo-reduction" of multiple iron centers by a single photon. This exciton effect leads to a splitting of the original localized transition. The 262 nm band is the low energy exciton branch; the high energy branch could be absent as a result of symmetry restrictions or it may be buried in the high background in the 220 nm region. The magnitude of an exciton shift is roughly proportional to the localized transition moments. Therefore, for the very intense charge transfer transitions, exciton shifts can be appreciable, whereas for the weak intrashell *d*-transitions these effects on the transition energy are negligible.

For iron (III) in tetrahedral coordination (phlogopite *A*, vermiculite), the charge transfer (oxo to Fe(III) is shifted to higher energies relative to the octahedral case. Lehmann (1970) observed similar relative positioning of the bands for these two oxo–iron (III) geometries; Schlafer (1955) observed the same trend for halogeno–iron (III) complexes. Jorgensen's "optical electronegativity" theory predicts just the opposite trend for the two geometries. On the other hand the electrostatic theory would predict the trend observed, since anion–cation distances in tetrahedral coordination are less than octahedral separations, but since this theory completely neglects directionality effects in bonding, the agreement may be fortuitous. It is possible that there is another much weaker charge transfer band in the 300 nm region but the spectra presented here show no real evidence to this effect.

Metal–metal transfer

In mineral systems containing appreciable amounts of Fe(II) or Ti(III) in the octahedral layer, several metal-to-metal charge transfer transitions are possible, all resulting in transitory "photo-oxidation" of these cations. Possible electron acceptors include Fe(III), Ti(IV), Al(III) and Mg(II). Intervalence transitions such as Fe(II)–Fe(III) and Ti(III)–Ti(IV) are of primary importance in determining the optical color properties of many minerals and have been investigated by several authors (Allen and Hush, 1967; Faye, 1968a; Faye and Nickel, 1970; Manning, 1968; Wehl, 1951). Because of the multitude of charge transfer transitions which can be stimulated by ultraviolet light, single crystals rich in Fe(II) or Ti(III) appear nearly opaque in the u.v. region; practically no spectral structure can be resolved. This is evidenced in biotite and to a lesser extent in muscovite and vermiculite. Transition energies are difficult to obtain theoretically; the assignment of these transitions is questionable. Table 5 contains a summary of transitions of this type along with approximate energies and systems in which they may have been observed.

The 250 nm band in chlorite, which Faye (1968, a) assigned to Fe(II)–Al(III) charge transfer could well be oxo–Fe(III) (octahedral) charge transfer; the transition energy is consistent with that observed for iron (III) substituted in other trioctahedral brucite-type layers.

Metal–ligand transfer

In systems containing octahedral iron (II), charge transfer involving electron migration from iron (II) to oxo ligands undoubtedly contributes to the intense background absorption in the u.v. region. The peak of the transition may lie in the vacuum u.v. but the low energy limb can contribute significantly to the intense background in the u.v. region studied here.

SUMMARY AND CONCLUSIONS

The qualitative evidence presented shows clearly that u.v.-visible spectroscopy can be of great value in clay mineralogy. As an analytical

Table 5. Metal to metal charge transfer summary

Transfer process	Max (nm) (approx.)	Clay mineral system	Reference
Fe (II) → Fe (III)	705	chlorite, biotite	Faye (1968, a), Faye *et al.* (1970)
Fe (II) → Ti (IV)	400	phlogopite	Faye (1968, a)
Fe (II) → Mg (II)	250	biotite (has not been assigned)	
Fe (II) → Al (III)	270	biotite	Faye (1968, a)
Ti (III) → Ti (IV)	450	tourmalines	

https://doi.org/10.1346/CCMN.1973.0210109 Published online by Cambridge University Press

tool, it provides a quick, nondestructive means of determining the presence (semi-quantitative), the site of substitution, and the valence state of the iron in the lattice. All clay minerals containing iron (III) (> 1 per cent) showed oxo–iron charge transfer in the u.v. region—octahedral iron (III) in the 240–262 nm range and tetrahedral iron (III) around 215 nm. Iron (III) intraconfigurational structure was evident in muscovite, vermiculite (transvaal), and nontronite. Iron (II) spectroscopic behavior defies generalization. Charge transfer is primarily of the metal–metal type which involves acceptor metal species that may be isomorphically substituted cations or the principal constituent cations of the host. The transition energy depends upon the acceptor species; minerals high in iron (II) usually show continuous charge transfer absorption throughout the visible and u.v. ranges. Iron (II) intraconfigurational structure in the visible region is masked by charge transfer absorption.

In addition to providing an iron fingerprint of the lattice, electronic spectra yield more specific information concerning the lattice environment contiguous to the iron. For a given ligand symmetry, the size of the lattice hole into which the iron cation fits can be inferred from the precise energy of the intraconfigurational and charge transfer bands. For octahedral Fe (III) systems, the relative hole size was found to be muscovite < nontronite < vermiculite.

Spectral splitting and bandwidths reflect the local ligand symmetry around the iron. Iron centers tend more toward regular geometry than the host lattice cations. At lower iron levels the iron geometry conforms to the crystallographic geometry of the host, showing some distortion from the regular symmetry, whereas, at high iron levels, i.e. in nontronite the iron dictates the layer geometry resulting in more regular local ligand symmetry.

Electronic spectroscopy gives insight into chemical as well as physical properties of clay minerals. Charge transfer is photonstimulated electron movement between nuclear centers. The energetics of similar electronic movement can be inferred from this spectral information.

The utility of the method has been established, but better spectra are needed. More detailed, resolved spectra could be obtained by employing micro techniques commonly reported in the literature. For the microcrystalline materials, low temperature (liquid nitrogen) should reduce spectral diffuseness by eliminating thermally activated coupling of molecular degrees of freedom.

Acknowledgment—The authors wish to thank Mr. Yewell Adams for technical assistance.

REFERENCES

Allen, G. C. and Hush, N. S. (1967) Intervalence transfer absorption: *Progr. Inorg. Chem.* **8**, 357.

Bailey, G. W., White, J. L. and Rothberg, T. (1968) Adsorption of organic herbicides by montmorillonite: Role of pH and chemical character of adsorbate: *Soil Sci. Soc. Amer. Proc.* **32**, 222.

Banin, A. and Lahav, N. (1968) Particle size and optical properties of montmorillonite in suspension: *Israel J. Chem.* **6**, 235.

Bowen, L. H., Weed, S. B., and Stevens, J. G. (1969) Mössbauer study of micas and their potassium depleted products: *Amer. Mineral.* **54**, 72.

Farmer, V. C. and Russell, J. D. (1967) Infrared absorption spectrometry in clay studies: *Clays and Clay Minerals* **15**, 121.

Farmer, V. C., Russell, J. D., and Ahlrich, J. L. (1968) Characterization of clay minerals by infrared spectroscopy: *Ninth Intern. Congr. of Soil Sci.* **3**, 101.

Faye, G. H. (1968,a) The optical absorption spectra of iron in six-coordinate sites in chlorite, biotite, phlogopite and vivianite: *Can. Mineral.* **9**, 403.

Faye, G. H. (1968,b) The optical absorption spectra of certain transition metal ions in muscovite, lepidolite, and fushsite: *Can. J. Earth Sci.* **5**, 31.

Faye, G. H. and Nickel, E. H. (1970) The effect of charge transfer processes on the color and pleochroism of amphiboles: *Can. Mineral.* **11**, 616.

Furlani, C. (1957) Spettri di assorbimento di complessi elettrostatici del Fe: *Gazz. Chim. Ital.* **87**(1), 376.

Jorgensen, C. K. (1962a) Chemical bonding inferred from visible and ultraviolet absorption spectra: *Sol. State Phys.* **13**, 376.

Jorgensen, C. K. (1962b) *Orbitals In Atoms and Molecules:* Academic Press, New York.

Lehmann, G. (1970) Ligand field and charge transfer spectra of Fe(III)–O complexes: *Z. Phys. Chem. Neue Folge* **72**, 279.

Lever, A. B. P. (1968) *Inorganic Electronic Spectroscopy*: Elsevier, New York.

McClure, D. S. (1963) Optical spectra of exchange coupled Mn^{2+} ion pairs in Zn Si Mn S: *J. Chem. Phys.* **39**, 2850.

Mortensen, J. L., Anderson, D. M., and White, J. L. (1965) Infrared spectrometry. In *Methods of Soil Analysis* (Edited by C. A. Black) Vol. 1, pp. 743–770, Am. Soc. Agronomy, Madison, Wisconsin.

Orgel, L. E. (1957) Ion compression and the color of ruby: *Nature* **179**, 1348.

Schlafer, H. L. (1955) Light absorption as a result of an interaction of two states of valency of the same element: *Z. Phys. Chem. Neue Folge* **3**, 222.

Taylor, G. L., Ruotsala, A. P. and Keeling, R. O. Jr. (1968) Analysis of iron in layer silicates by Mössbauer spectroscopy: *Clays and Clay Minerals* **16**, 381.

Weaver, C. E., Wampler, J. M. and Pecuil, T. E. (1967) Mössbauer analysis of iron in clay minerals- *Science* **156**, 504.

Wehl, W. A. (1951) Light absorption as a result of interaction of two states of valency of the same element: *J. Phys. Coll. Chem.* **55**(1), 507.

White, J. L. (1971) Interpretation of infrared spectra of soil minerals: *Soil Sci.* **112**, 22.

Résumé – Un tour d'horizon préliminaire des spectres d'absorption électronique des minéraux argileux révèle l'utilité de la spectroscopie ultraviolet-visible si l'on veut élucider les propriétés structurales, physiques et chimiques de tels systèmes. Les spectres, obtenus avec des suspensions, des films ou des monocristaux (quand c'est possible) sont interprétés en terme de transitions associées au fer. Les minéraux argileux microcristallins montrent d'une façon typique le Fe (III) dans une géométrie octaédrique d'oxo-ligands, tandis que les minéraux du type mica peuvent montrer toute une série d'espèces du fer, comprenant Fe (III) octaédrique, Fe III tétraédrique et Fe (II) octaédrique. Le fer affecte la géométrie locale du site et dans les minéraux "riches en fer" peut imposer une géométrie au feuillet et pàr là, imposer la forme cristalline.

Kurzreferat – Eine Voranalyse der elektronischen Absorptionsspektren von Tonmineralien erweist den Wert ultraviolett-sichtbarer Spektroskopie für die Erforschung der strukturellen, physischen und chemischen Eigenschaften derartiger Systeme. Spektren, die in den Suspensions-, Film- und Einkristallzuständen (je nach Verfügbarkeit) erzielt wurden, werden als Übergangsphasen in Verbindung mit Eisen interpretiert. Mikrokristalline Tonmineralien weisen typisch Fe(III) in oktahedralem Oxoverband auf, während glimmerartige Mineralien eine Reihe von Eisenarten wie oktahedralem Fe(III), tetrahedralem Fe(III) und oktahedralem Fe(II) enthalten mögen. Eisen übt auf die lokale Lagerstättengeometrie einen Einfluß aus und kann in eisenreichen Mineralien für die Schichtengeometrie und daher die Kristallform entscheidend sein.

Резюме — Предварительное исследование спектра электронного поглощения глинистых минералов выявило ценность видимой ультрафиолетовой спектроскопии в разъяснении структурных физических и химических особенностей таких систем. Спектры полученные от суспензии, на пленке и на сростке отдельных кристаллов (где относится) расшифровывались как соединения с железом. Микрокристаллические глинистые минералы обычно включают Fe(III) в восьмигранной оксо-лигиндной конфигурации, в то время как слюдистые минералы могут состоять из ряда железистых групп, включая октаэдральный Fe(III) тетраэдральный Fe(III) и октаэдральный Fe(II). Железо влияет на конфигурацию места заложения и в минералах с высоким содержанием железа оно может влиять на конфигурацию слоев и на форму кристаллов.

https://doi.org/10.1346/CCMN.1973.0210109 Published online by Cambridge University Press